Dispersion Measurements of AlGaAs Microring Resonators

Project Authored by

Caroline Munck Nielsen

Student ID: kvc457

E-mail: kvc457@alumni.ku.dk

Under Supervision by

Jan W. Thomsen

Head of Institute, Niels Bohr Institute

E-mail: head_of_institute@nbi.ku.dk

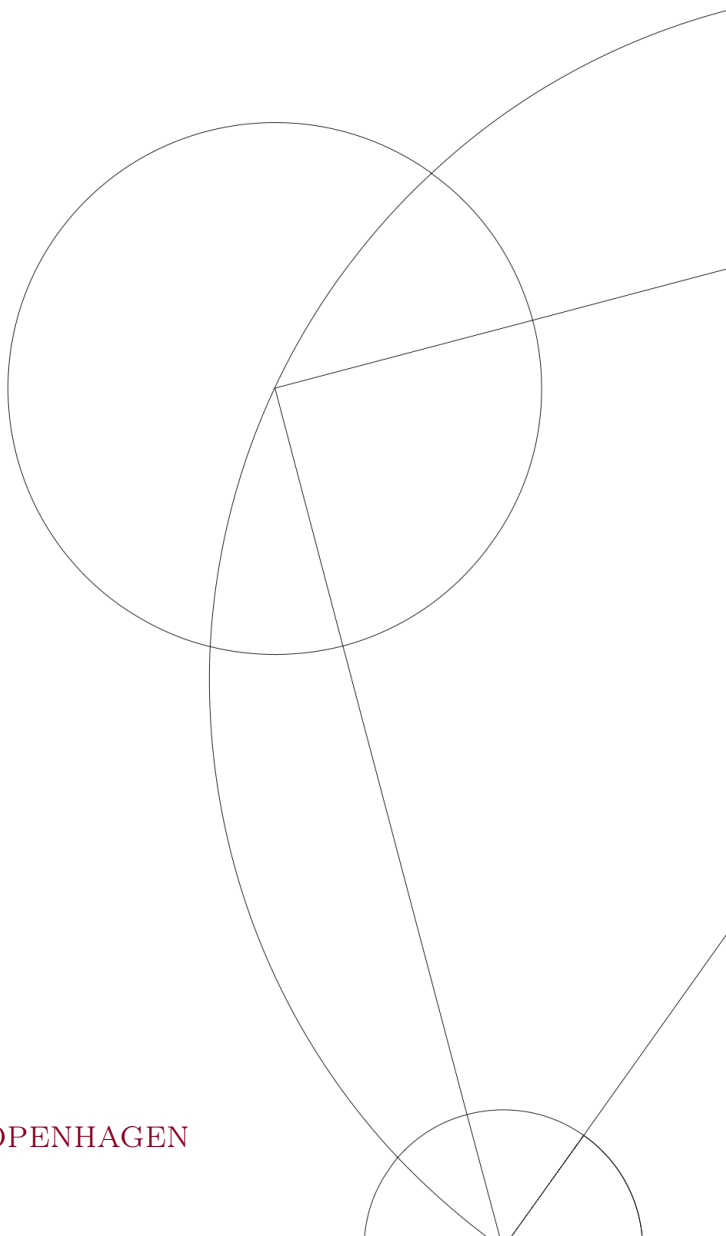

University of Copenhagen

Abstract

There has been an increasing interest in frequency comb in the resent years but the commercial frequency combs are very expensive and cumbersome. Newer and better ways of creating the combs are therefore on a rise. This report gives a brief introduction to the most fundamental theory, and investigates different ways of measuring and determining the dispersion of AlGaAs microring resonators with the possibility of comb generation in the future. Two methods are presented and compared. The first method uses the spectral lines of an acetylene $^{13}C_2H_2$ gas cell as a way to determine the dispersion of the microresonator. The other method exploit the properties of a Fabry-Pérot interferometer as a way to determine the dispersion. In both setups we found the dispersion to be anomalous with values around -10^3 fs^2/mm for acetylene and -10^{-2} fs^2/mm for the Fabry-Pérot interferometer.

Resumé

Der har været en stigende interesse indenfor frekvenskamme de sidste par år, men de nuværende frekvenskamme er både dyre og upraktiske. Derfor er mange begyndt at lede efter nyere og bedre måder, hvorpå man kan generere frekvenskamme. I dette projekt vil der kort blive redegjort for den mest fundamentale teori indenfor området, hvorefter forskellige måder hvorpå, man kan måle og bestemme dispersionen i en AlGaAs mikroringsresonator, er blevet undersøgt med henblik på mulig generering af en frekvenskam, på et senere tidspunkt. To forskellige metoder er blevet præsenteret og sammenlignet. Den første metode benytter sig af spektrallinjerne i en $^{13}C_2H_2$ acetylen-celle til at bestemme dispersionen af mikroresonatoren. Den anden metode udnytter egenskaberne ved et Fabry-Pérot interferometer til at bestemme dispersionen. I begge opstillinger er dispersionen fundet til at være anormal med værdier omkring -10^3 fs^2/mm, for acetylene og -10^{-2} fs^2/mm for interferometeret.

Acknowledgements

First I would like to thank my supervisor Jan W. Thomsen for taking the time to supervise this project even though time is not on his hands at the moment. His enthusiasm towards this project has been highly appreciated. Also, Martin Romme Henriksen and Arvad Asbjørn Jørgensen both deserves an enormous thank for all the work and effort they put into this project, helping me when needed. This project would not have been the same without their help and patience. I would also like to thank Stefan Alaric Schäffer, Lars-Emil Gutt and Mikkel Tang for taking their time to help me in the lab and for proofreading my bachelor thesis. At last, I would like to thank Andreas Berglund for the help he provided with MATLAB when in need and also Anja Andersen Cawley for proofreading in the final hours.

Contents

1 Introduction

Since Roy J. Glauber, John L. Hall and Theodor W. Hänsch won the Nobel prize back in 2005 there has been an immense increase of interest in the field of frequency comb generation.

The frequency comb is essentially a laser, but instead of only a very narrow range of frequencies, the optical frequency comb is a broadband laser consisting of a spectrum of coherent and evenly spaced frequency components. This property is what makes it so useful as it can be used as an optical ruler, making it an incredibly interesting area of research. The frequency comb can be applied many in different areas such as laser stabilization, coherent optical communication, short pulse generation, radio frequency signal processing and frequency metrology [2].

The commercial comb already exists [1] but the existing combs are impractical due to their current high pricing and power consumption but also shear size. It would therefore be preferable if a smaller low cost version could be realized.

1.1 Optical Frequency Comb Generation in Microring Resonator

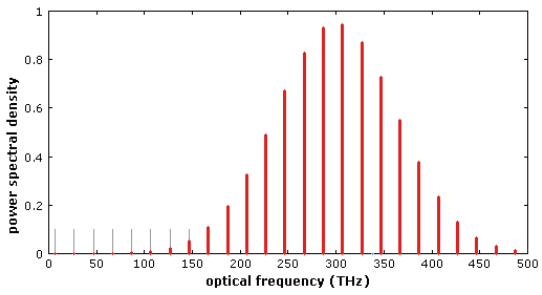

Figure 1: An example of an ideal frequency comb [5] consisting of a carrier frequency, ν_0 and equidistant lines with a modulation frequency of ν_n.

The lines of the comb are created through the pumping of a resonator with a continuous-wave laser. The comb is the result of the nonlinear interaction between the light of the laser and the optical resonator [3], and ideally they would obtain the form of delta functions separated by the exact same frequency. The distance between two consecutive lines in a comb would correspond to the free spectral range (FSR) of the microresonator. The frequency comb comes from the Fourier transform of train pulses in the time domain. In the frequency domain this becomes the teeth of the comb.

Nonlinear effects can cause the carrier-envelope offset to slip, meaning that the electric field is shifted with respect to the envelope. The carrier-envelope offset occurs due to fluctuation in the phase of the pulse train. If the offset of the wave envelope is constant the frequency of the nth comb line could be written as [5]

$$\nu_n = \nu_{ceo} + n \cdot f_{rep}, \tag{1}$$

where ν_{ceo} is the carrier-envelope offset frequency, n is an integer ($n = 0, 1, 2, ...$) and f_{rep} is the repetition rate of the train pulse, i.e. the spacing between the comb lines. If the pulse train was perfectly periodic the frequency of the lines of the comb would be equidistant described by the pulse repetition rate [5].

1.2 This Project

This project seeks to investigate the possibilities of generating a frequency comb using an AlGaAs microresonator chip, exploiting the strong second and third order nonlinear effects exhibited in the material. Scanning the resonator over a reasonable range of wavelengths will show a change in the group velocity dispersion (GVD) in the material due to AlGaAs' refractive index's wavelength dependency. The anomalous GVD is an essential property of the microresonator when generating a frequency comb. This is because when the microresonator is being pumped by a continuous-wave laser, equidistant lines can appear as a result of four wave mixing (FWM).

The goal of the project is to map the dispersion of an AlGaAs microresonator using two different methods: One way is to use a wavelength reference obtained from a molecular spectrum, in this case the spectrum of the gas *acetylene* ($^{13}C_2H_2$). The other way is to use a cavity with a known free spectral range (FSR) and very little dispersion. For this we build a *Fabry-Pérot interferometer* with a known FSR value of 175.3 MHz.. When the laser scans the microresonator the resonances and the FSR are measured in a scan time. The references is used to calibrate the measurements from scan time in seconds to frequency in Hertz. This is necessary as we cannot assume our laser to be scanning perfectly linearly. By analyzing measurements from the two setups, using the two above mentioned methods for calibration, we look for an optimal way of mapping the dispersion of the AlGaAs microresonator.

2 Theory

2.1 Nonlinear Optical Dynamics

2.1.1 Nonlinear Effects of Comb Generation Dynamics

The nonlinearity can be seen in the polarization of a material

$$\overline{P} = \varepsilon_0(\chi^{(1)} \cdot \overline{E} + \chi^{(2)} \cdot \overline{E}^2 \chi^{(3)} \cdot \overline{E}^3 + ...). \tag{2}$$

This is a power series of the polarization $\overline{P}$ where $\overline{E}$ is the applied optical field and ε_0 is the vacuum permitivity. $\chi^{(j)}$ $(j = 1, 2, ...)$ is the jth order susceptibility given by a tensor of rank $j + 1$. First order susceptibility is known as the linear susceptibility with $\chi^{(1)}$ as the linearity constant between the polarization and the applied field [3] and can be written as

$$\begin{pmatrix} P_x \\ P_y \\ P_z \end{pmatrix} = \epsilon_0 \begin{pmatrix} \chi_{xx} & \chi_{xy} & \chi^{xz} \\ \chi_{yx} & \chi_{yy} & \chi_{yz} \\ \chi_{zx} & \chi_{zy} & \chi_{zz} \end{pmatrix} \begin{pmatrix} E_x \\ E_y \\ E_z \end{pmatrix}. \tag{3}$$

$\chi^{(2)}$ and $\chi^{(3)}$ are the second and third order susceptibility, respectively. The second order nonlinearity is accountable for ex. second-harmonic generation, frequency doubling and sum/difference frequency generation. The most interesting for this experiment is the third order susceptibility, $\chi^{(3)}$ as it is responsible for effects such as the Kerr effect, third

harmonic generation, four-wave mixing and two-photon absorption.

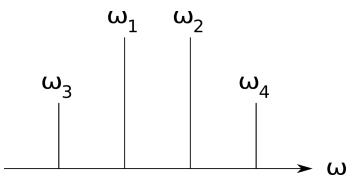

Figure 2: Illustration of FWM.

The most fundamental of the aforementioned nonlinear processes in frequency comb generation is the four-wave mixing (FWM). It occurs when the microresonator is pumped with high intensities and the effect is characterized by two pump photons coming together to produce a photon pair of new frequencies such that net energy and momentum are conserved in the process,

$$\omega_{1,p} + \omega_{2,p} = \omega_3 + \omega_4, \tag{4}$$

where $\omega_{1,p}$ and $\omega_{2,p}$ are the pump frequencies and ω_3 and ω_4 are the new photon pair. The two pump photons, $\omega_{1,p}$ and $\omega_{2,p}$ can either be of same ($\omega_{1,p} = \omega_{2,p}$) or different ($\omega_{1,p} \neq \omega_{2,p}$) frequencies, making the process, respectively, degenerate or non-degenerate. Since the a monochromatic continuous wave laser is used in this experiment, the initial FWM must be degenerate. The FWM will give rise to several oscillating modes creating the teeth of the Kerr frequency comb.

2.1.2 Group Velocity Dispersion

The nonlinear effects needed in the generation of a frequency comb are highly dependent on the group velocity dispersion (GVD). The group velocity is what characterizes the velocity at which the envelope of a wave-packet propagates through a medium. In our case the medium is the AlGaAs microresonator. AlGaAs is a semiconductor, making it a dispersive material. This means the refractive index, n of the material is wavelength dependent and will therefore create dispersion of the envelope, the GVD. There are two forms of dispersion, normal and anomalous. The latter is needed for the comb generation. Anomalous dispersion is required to obtain parametric gain in the nonlinear processes described by (4) [6]. Parametric gain is an optical process in which a signal can be amplified in a nonlinear material such as AlGaAs, when interacting with a photon of a different frequency [15]. The dispersion of a microresonator such as AlGaAs, used in this experiment, can be described using the Taylor expansion of the dispersion law [7]

$$\omega_\mu = \omega_0 + D_1\mu + \frac{1}{2}D_2\mu^2 + \frac{1}{6}D_3\mu^3 + ..., \tag{5}$$

using the resonance frequency, ω_μ with μ denoting the relative mode number with respect to the pump laser, denoted $\mu = 0$. For this experiment we have chosen the mode closest to 1542 nm to be $\mu = 0$. The parameters $D_1, D_2, D_3, ...$ are all related to the order of dispersion, D_1 being the FSR and the two others being the second and third order dispersion parameters, respectively. The second order dispersion parameter is related to the GVD parameter β_2 through [7]

$$D_2 = -\frac{c}{n}D_1^2\beta_2, \tag{6}$$

Where c is the speed of light and n is the index refraction at a given wavelength. Furthermore, it should be noted that anomalous dispersion would be indicated by a positive value for D_2.

2.2 Optical Cavity

The idea behind an optical cavity is to "trap" light, such that you allow a beam of light to travel back and forth in a closed path inside the cavity [8]. Even though there are many different ways of constructing an optical cavity (or optical resonator) the fundamentals are the same. The cavity can only support wavelengths where standing waves are created. These standing waves are caused by constructive interference at certain resonance frequencies and are called the longitudal modes. Longitudal mode patterns has the nodes along the length of the cavity. For a simple free space cavity the frequencies of the longitudal modes are dependent on the length of the cavity through the relation

$$\nu = m\frac{c}{2nL}, \tag{7}$$

where $m = 1, 2, 3, ...$ is an integer related to how many nodes there are. Transverse modes (or transverse electromagnetic mode (TEM)) can also appear with nodes perpendicular to the length of the cavity. The output of a laser beam is Gaussian, meaning that the most focusable beam is the one that will have the lowest mode, i.e. TEM00 which is also Gaussian.

For this project two types of cavities have been used. The waveguide on the AlGaAs micro-resonator is a ring cavity. The other type of cavity used in the setup is a Fabry-Pérot interferometer. This cavity will be used as a reference due to is relatively small free spectral range.

2.2.1 Ring Cavity

The ring cavity (alternatively resonator) is a fiber cavity. It works by passing a fiber close by a ring of radius, R. If the fiber and the ring cavity are close enough to each other the electric field propagating through the fiber can be transmitted to the ring cavity through a phenomenon known as evanescent coupling.

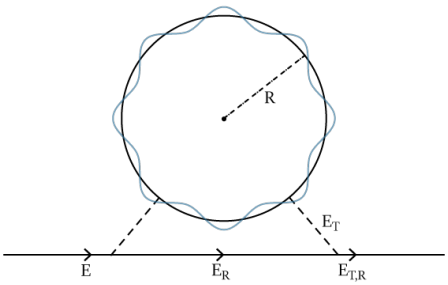

Figure 3: **Illustration of a ring cavity with a radius, R**. As the E-field propagates close to the ring cavity some of the light will couple to the cavity. Each time the light passes by the fiber again, some of the light is transmitted, E_T. The light continuing to propagate in the fiber, without coupling to the cavity, is the reflected light E_R.

If the light is coupled from the fiber to the ring, the light will then propagate along the ring. Every time the light has made one round it passes the fiber again and when it does it will either be transmitted back to the fiber or continue to propagate in the ring, as illustrated in Figure 3.

2.2.2 Free Spectral Range

The free spectral range (FSR) is a term related to an optical cavity describing the range in frequency between two resonator-modes. For an air filled free space cavity, the FSR can be approximated to be

$$FSR = \frac{c}{2nL}, \tag{8}$$

where c is the speed of light and L is the length of the cavity [9]. Alternatively, when using a ring cavity, the light only has to travel one round, so the FSR is instead given by

$$FSR = \frac{c}{nL}. \tag{9}$$

The important thing here is that the phase of the light is identical to the new incoupled light, as it is constructive interference. The difference of the factor 2^{-1} is because for the free space cavity the standing waves have to match to two nodes, whereas for the ring cavity they only need to be able to stand around the ring, i.e. a single node.

Besides this, the finesse of a free space cavity can be can be calculated using the relation (for R<0.5)

$$F = \frac{\pi\sqrt{R}}{1-R}, \tag{10}$$

where R is the reflectance of the mirrors used to build the cavity.

The main objective is to examine whether or not the dispersion of a microresonator can be determined by measuring the change in the FSR when scanning over a range of wavelengths.

3 Experimental Setup

The main setup revolves around the AlGaAs microring resonator from which the GVD is to be determined. The AlGaAs microring is constructed in such a way that when a waveguide is running very close to the cavity, the light from the waveguide can couple into the resonator. This is called evanescent coupling. The resonance frequency of the cavity will be determined by the optical path length (OPL). A schematic overview of the setup can be seen in Figure 4.

The light from the laser is split using a fiber splitter, which divides the signal into 50%/50%. One part is to be sent through the microresonator and the other through the reference (A) or (B). The light going to the microresonator is sent through an attenuator to reduce the power of the light. The light is then split into two components. 1% of the light is used to measure the input power, P_{in}. The remaining 99% is sent through a polarization controller and then further on into the microresonator. After the microresonator, the light is once again divided into 1% and 99%. 1% is used to measure the output power, P_{out} and

the remaining 99% is measured by a photo detector, showing the light of the transmission through the microresonator. The other part of the 50/50 light either goes to (A) or (B). In (A) the light is sent through a plano convex lens and is bounced back and forth inside a cell containing the acetylene and again on the other side where the transmission light is detected by a photo diode. In (B) the light is once again split using a fiber splitter into 50/50. One part goes through a fiber cavity and into a photo diode and the other part goes to the Fabry-Pérot interferometer.

It is to be noted that the tunable laser used in setup (A) and (B) is not the same. In (A) a Santec tsl-710 laser with a wavelength range of 1510 nm to 1555 nm was used and in (B) a Toptica DLC (Digital Laser Controller) pro was used, which has a wavelength coverage of 1520 nm to 1630 nm. Both lasers are external cavity diode laser (ECDL) with a build-in piezoelectric element to help change the wavelength of the laser, so it can be used to scan over a range of wavelengths.

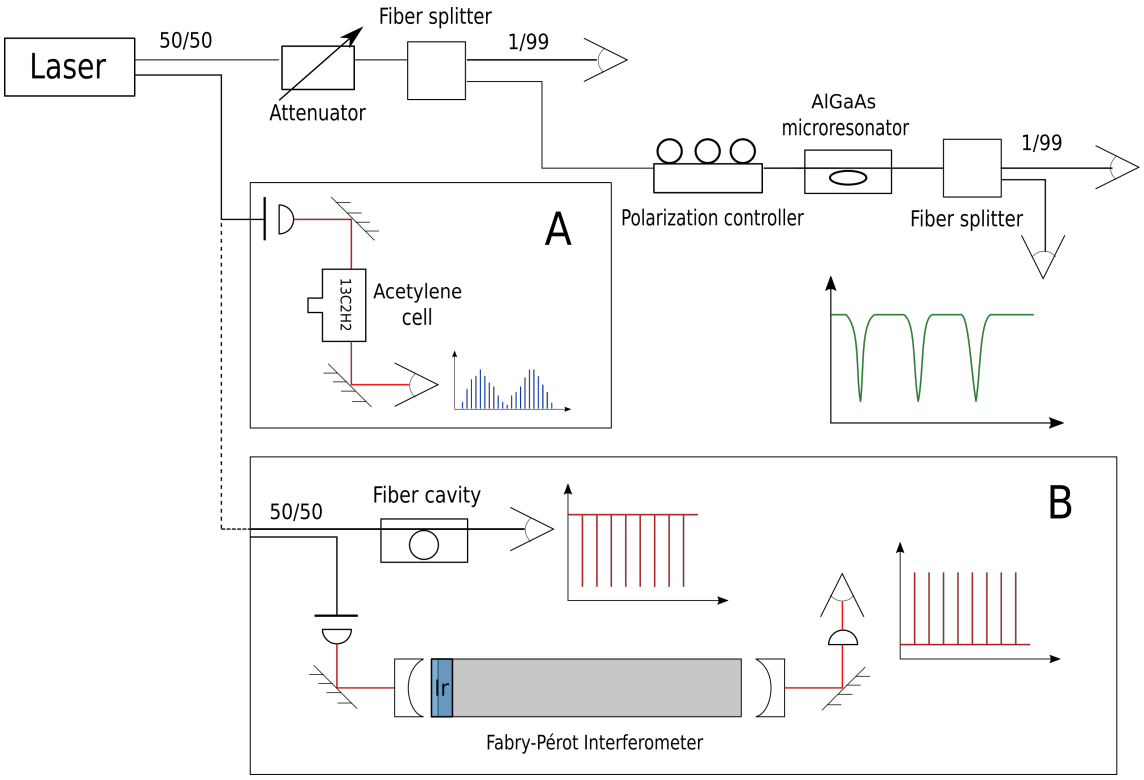

Figure 4: **Schematic overview of the experimental setup**. Full black lines are optical fibers and the red lines are free space laser light. PD: Photodiode, pcx: plane convex, Ir: iris. Fiber splitters are used to divide the specified amount of light in each direction. The setup is divided into two sub-setups (A) and (B). (A) First part of the experiment uses an acetylene gas cell as reference and (B) is the second part of the experiment with a Fabry-Pérot interferometer as reference.

3.1 The AlGaAs Micro-ring Resonator

The ring cavity used in this experiment is a microresonator based on an $Al_{17}Ga_{83}As$ (aluminum gallium arsenide)-on-insulator (AlGaAsOI) platform. In the recent years the interest in AlGaAs has been increasing as a possible and promising candidate for replacing silica nitride (Si_3N_4) in waveguide development. Both materials are known for their high nonlinearity, which is necessary in the generation of frequency combs. Moreover, AlGaAs exhibits strong second and third order nonlinear effects, due to its non-centrosymmetric crystal structure, which gives a high linear refractive index as well as low nonlinear loss. A non-centrosymmetric structure refers to the structure of the crystal not having a symmetric inversion, which means that the overall symmetry does not exhibit symmetry. The effective nonlinearity of AlGaAs is orders of magnitude higher than that of Si_3N_4, making it more effective in the potential generation of a frequency comb. [10].

The ring selected for measurements in this experiment is waveguide number 83 on the CG49 chip. The CG49 is made by DTU Fotonik and consists of a thin layer of AlGaAs on top of a layer of insulator that resides on a semiconductor substrate. The dimensions of the waveguide can be seen in Table 1.

Table 1: Dimensions of WG83

Microring 83					
L_{ring} [μm]	W_{bus} [μm]	W_{nrw} [nm]	W_{wide} [nm]	R_n/W [%]	Gap [nm]
2058	480	480	800	15/15	500

The CG49 is an AlGaAsOI platform with an aluminium fraction (x) of 17 %, resulting in an effective refractive index of $n = 3.3481$ at 1542 nm. The refractive index can be calculated using the procedure found in [11].

4 Measurements

We have been pumping the microresonator on the AlGaAsOI with a continuous wave laser scanning over a range of wavelengths. Using the two different setups described in 3 we took a number measurements and tried to determined the value of the dispersion of the microresonator by measuring the FSR of the selfsame.

4.1 Acetylene Reference Cell

In this setup, (A), the laser scanned over the microresonator in the interval 1510 nm to 1550 nm. We took measurements for 25 nm/s, 50 nm/s, 75 nm/s and 100 nm/s with ten datasets for each scan speed. In figure 5 a typical scan with the laser through the microresonator can be seen.

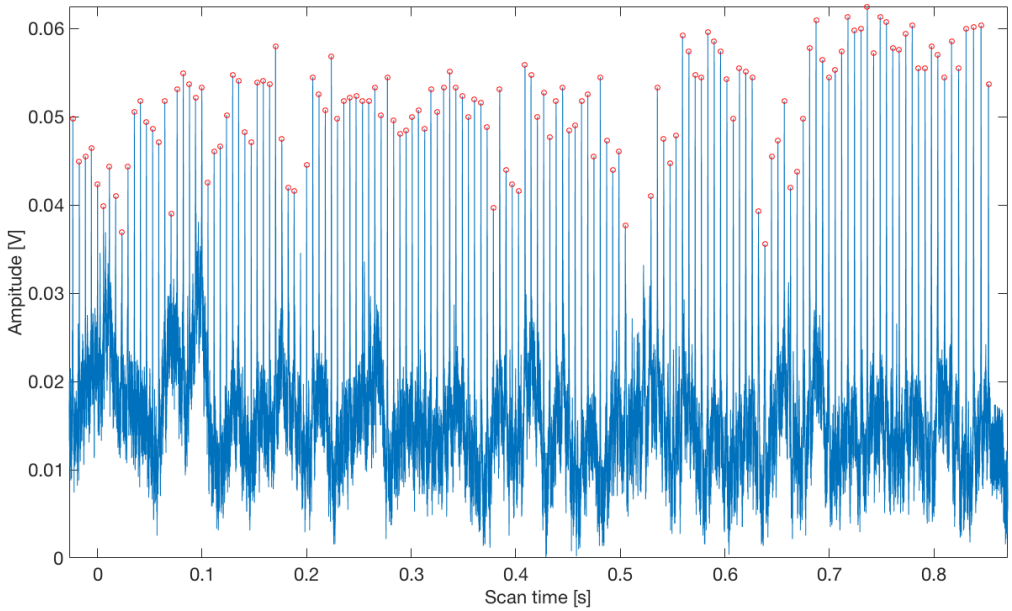

Figure 5: **Scan through the microresonator** at 50 nm/s. On the x-axis we have the time of the oscilloscope relative to the trigger point in seconds [s] and on the y-axis the amplitude of the resonance in volt [V]. The red circles mark the peak in each resonance. The resonances have been normalized to make it more convenient to locate the peaks.

.

To map the dispersion of the excited waveguide we need to know the FSR related to the resonances in the ring. Since the FSR is measured in frequency, we need a way to calibrate the time axis in which the oscilloscope returns the data. For this, a reference with known values at certain points is needed.

In this experiment the x-axis was calibrated using a cell containing the molecular gas acetylene $^{13}C_2H_2$. The advantage of using acetylene is that the optical frequencies of the absorption lines are known with great certainty around the C-band (1530 nm to 1565 nm) of optical telecommunication [12]. The absorption spectrum of the $\nu_1+\nu_3$ band of acetylene range from 1516.6 nm to 1532.8 nm for the R-branch and 1533.8 nm to 1558.8 nm for the P-branch.

A list of the values of the absorptions lines can be found in Appendix A [13]. Scanning through the microresonator and the gas cell simultaneously, it was possible to use the absorption lines of the molecule as a way of converting the relative time axis. Making an estimate of the new wavelength axis based on the start value of the scan interval, and assuming a perfectly linear scan speed throughout the scan. This new axis was then used to match the mea-

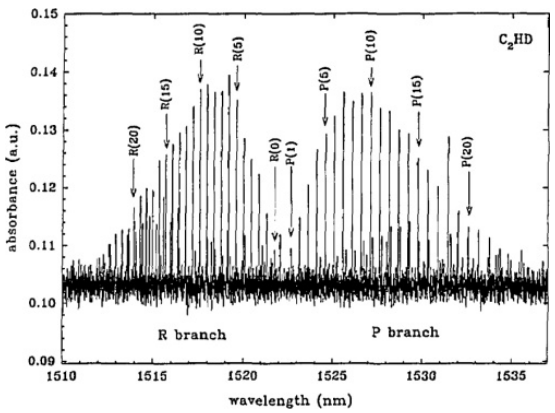

Figure 6: The spectrum of the $\nu_1 + \nu_3$ band of acetylene, $^{13}C_2H_2$ [14].

sured absorption lines of the cell with the
reference values. A typical scan through the gas cell and the lines of reference can be seen in Figure 7.

The lines of the cell and reference were matched using an interval condition. In order for a peak of the cell to be matched to a reference value it was not to deviate more than ± 0.06 nm from a line of reference. To make sure that the correct lines were matched to the references, and that the measured absorption lines were not shifted by an incorrect offset value, a further analysis of the top two peaks of each branch were conducted. The reason for this was to determine whether or not one of these peaks could be matched with the R(10) or P(10) absorption line. The tenth line of both the R- and P-branch of acetylene's spectrum is the one with the highest absorbency making it the highest in the spectrum as seen in Figure 6. This makes it easier to locate over the other absorption lines.

When the peaks of the cell have been matched to a reference value the true value of each peak is then known, namely the reference value. Assuming the laser is scanning linearly between two reference peaks, the distance between each peak value is then linearly interpolated using the adjacent peak values. Hereby, a new axis with the same number of data points is created containing all the wavelengths. Converting the wavelength axis to a frequency axis is easily done using the relation, $f = \frac{c}{\lambda}$, where c is the speed of light [1].

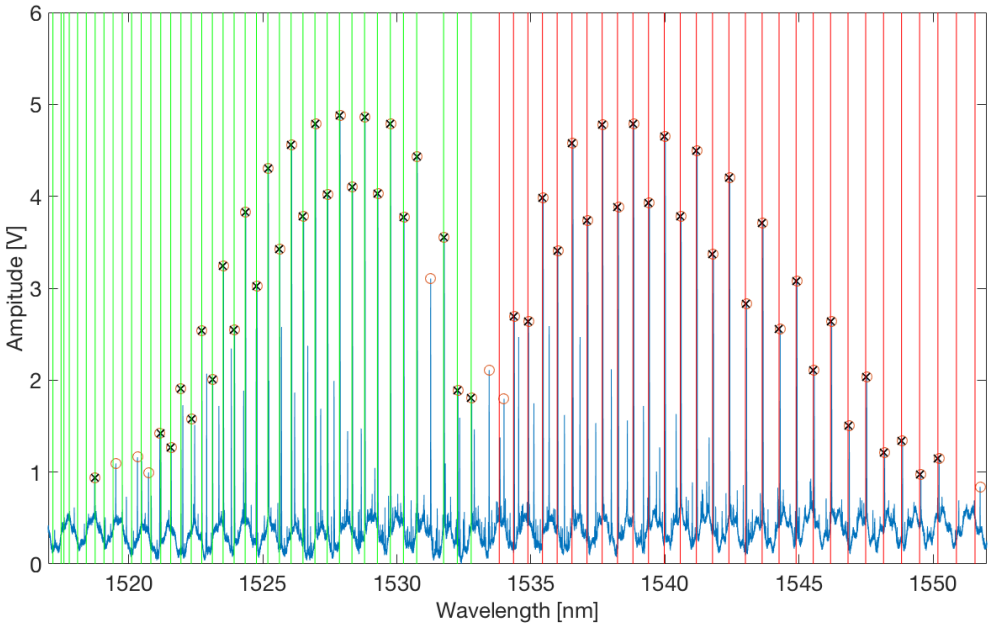

Figure 7: **Scan through the gas cell** at 50 nm/s. The x-axis show the temporary wavelength axis [nm] and the y-axis shows the amplitude of the absorption in volt [V]. The data shown in blue is the scan through the gas cell. The green and red vertical lines represent the R- and P-branch reference values, respectively. The black crosses marks where a scan peak have been match to a reference value. The data have been normalized for convenience.

.

[1]The value of the speed of light is here set to be $c = 2.9979 \cdot 10^8$ m/s

After the axis is converted the data from the scan through the microresonator is plotted against the new frequency axis. The distance between each peak is then determined with respect to the new axis and the FSR in frequency is found (see Figure 8).

In order to determine the value of the GVD parameter β_2, defined in 6, we need the values for the first and second order dispersion, D_1 and D_2. Both these parameters are related to the FSR and the mode number (or alternatively the wavelength) of the resonances. The numbering of the modes are somewhat arbitrary as they are points which we choose. In this case we choose the mode closest to 1542 nm as the zeroth mode.The remaining resonances are then numbered after using integers $n = \pm 1, \pm 2, \pm 3, ...$ on each side of $\mu = 0$.

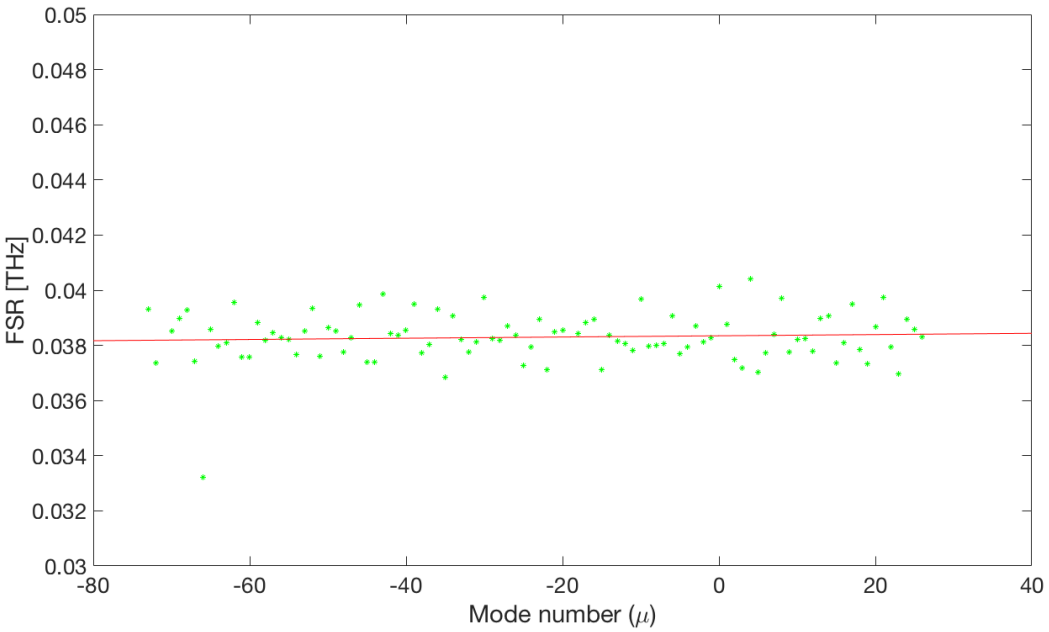

Figure 8: **FSR as a function of mode number** μ at 50 nm/s for a single scan. On the x-axis the mode numbers centered around the $\mu = 0$, located at 1542 nm, are plotted. On the y-axis we see FSR in THz. The red line is a fit of the included data points marked by green crosses. Data points which are more than 0.5 THz from the mean are excluded.

.

The values found for FSR is plotted as a function of the mode number. The data points are fitted using a linear fit, $ax + b$. This linear fit is used to tell whether or not the dispersion in the AlGaAs microresonator is anomalous. A representative plot of a single scan can be seen in Figure 8. The mean values of D_1, D_2 and GVD for each scan speed can be found in Table 2.

Table 2: Results

	$\mathbf{D_1}$ **[rad/s]**	$\mathbf{D_2}$ **[rad/s]**	β_2 **[fs^2/mm]**
25 nm/s	$2.4835 \cdot 10^{11} \pm 4.6719 \cdot 10^{8}$	$(0.4028 \pm 8.3184) \cdot 10^{7}$	$-818.1960 \pm 9.4668 \cdot 10^{4}$
50 nm/s	$2.4880 \cdot 10^{11} \pm 6.5870 \cdot 10^{8}$	$(1.0649 \pm 3.9255) \cdot 10^{7}$	$-1.9135 \cdot 10^{3} \pm 4.4512 \cdot 10^{4}$
75 nm/s	$2.6646 \cdot 10^{11} \pm 6.1259 \cdot 10^{8}$	$(0.8071 \pm 3.4539) \cdot 10^{7}$	$-1.3842 \cdot 10^{3} \pm 3.4146 \cdot 10^{4}$
100 nm/s	$2.3832 \cdot 10^{11} \pm 5.6284 \cdot 10^{8}$	$(0.6904 \pm 3.6228) \cdot 10^{7}$	$-1.3566 \cdot 10^{3} \pm 4.4773 \cdot 10^{4}$

D_1, the first order dispersion value, is the FSR value at $\mu = 0$. The second order dispersion value, D_2 is the slope of the fit. D_2 is assumed to be positive in all cases, because this means the GVD is anomalous. The uncertainties of the peaks of the measured resonances is found by fitting a Lorentzian curve to each one of them. By applying the standard uncorrelated error propagation, the uncertainty of the parameter D_1 is found, while the uncertainty on D_2 is given by the fitting parameters of the linear fit to the FSR. Finally, the uncertainty on the GVD, β_2 is also found by error propagation.

For each of the different scan speeds, a total number of ten measurements were conducted. In Figure 9 the standard deviation of each of the ten scans can be seen for the four different scan speeds. Here, we see that the standard deviation does deviate from each scan, but only within a very small area of roughly $1 * 10^{-4} - 2 * 10^{-4}$ THz. Furthermore, in Figure 10 we see a box plot of the residual values. From this plot we can see that the scan speed does not have a great influence on the variance of FSR values, as also implied by Figure 9. However, one could argue that for a scan speed of 100 nm/s there seems to be a bit more variance in the results for the FSR values.

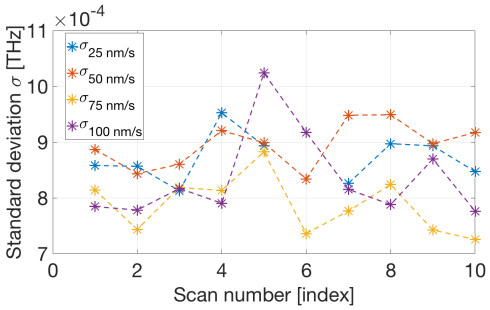

Figure 9: **Standard deviation of the residuals** of the FSR compared to the linear fit for one single scan. For each of the four scan speeds, the standard deviation of the ten scans is plotted as a function of the scan number going from 1-10. Note that one of the scans for 25 nm/s have been left out and is therefore not showing on the plot.

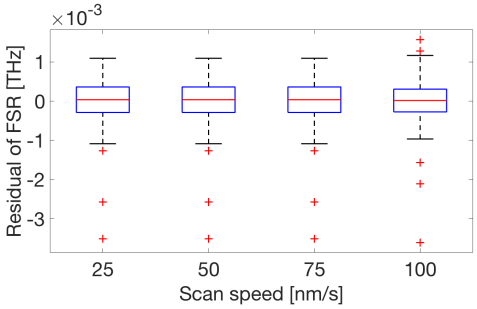

Figure 10: **Box plot of the mean residual value** for each mode at the different scan speeds. The red lines indicate the mean value of the residual and the blue box marks the upper and lower quantile of the data points. The black lines are the maximum and minimum values. The red crosses are single outliers.

4.2 Fabry-Pérot Interferometer Reference

Although the acetylene cell provided a good reference with well known values, the distance between each reference point is quite large. The problem is, that there are too few reference points to scale the frequency axis by. For the acetylene cell we obtained only roughly 30 lines over a range of 50 nm but building a cavity as the Fabry-Pérot interferometer we can achieve much smaller spacing between each point.

The Fabry-Pérot interferometer is a free space cavity. This type of linear cavity can be build in such a way that it will have sharp resonances with small spacing in between each resonance. For this type of cavity the FSR is given by equation (8). The cavity length used in this experiment is 82 cm, which would give a theoretical value of $FSR = 182.3$ MHz. With a FSR of that order we instead obtain around 69,000 resonances over a range of 100 nm. The assumption that the laser is linear between two resonances is justified more in this case.

4.2.1 Building and Optimizing the Cavity

The cavity itself consists of a 82 cm long aluminium profile with a mirror placed at each end of it. The mirrors used have a radius of curvature (RoC) of 9000 mm and a reflectance of 99.99%. At the beginning of the cavity, an iris is placed right after the mirror. This is done in order to eliminate higher order modes, so that TEM00 will be the most prominent mode. The TEM00 mode is desirable due to its gaussian beam shape which means that it has the highest intensity in the center of the beam profile making it easier to work with and align.

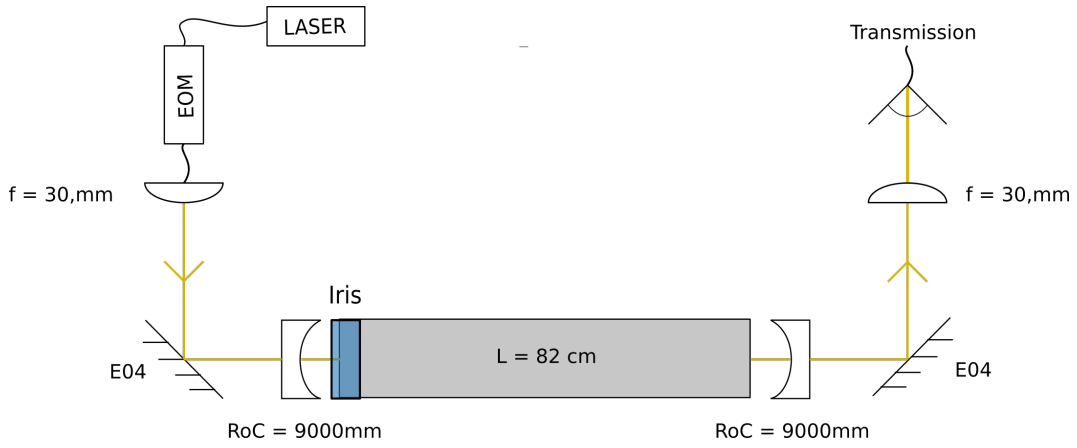

Figure 11: **Setup of the Fabry-Pérot Cavity**. A laser connected to a piezo is directed through an EOM to create sidebands. This signal with the sidebands is send through a plane convex lense to collimate the beam. The beam is reflected on a mirror and into the cavity. On the other side it is once again reflected and focused onto a photo diode by focusing the beam with another plane convex lens.

.

The initial signal from the laser is sent through an EOM (Electrico Optical Modulator) to create sidebands on each side of the resonance frequencies, $\omega \pm \Omega$. By tuning the frequency

of the sidebands, the FSR of the cavity can be determined. The FSR of the cavity will be equal to the sideband frequency when a sideband belonging to a neighboring resonance overlap with the resonance being looked at. Using this method the FSR was determined to be 175.3 MHZ, which is with good correspondence to the theoretical value of 182.3 MHz.

From the EOM the beam of light is collimated using a plane convex lens with a focal length of 30 mm. From the lens the collimated beam is reflected on a mirror and into the cavity. On the other side of the cavity the light is reflected once again and sent through another plane convex lens with the same focal length as the first. This lens is used to focus the beam of light before it is detected by the photo diode.

Due to the very high reflectance of the mirrors the finesse of the cavity is extremely high compared to what would be the ideal. Even though, the exact finesse has not been calculated, it is estimated to be around 30,000 using equation (10). With a finesse of that order it is extremely difficult to determine the FSR of the cavity because of higher order modes being present. To overcome this problem the iris was added to the aluminum profile, see Figure 4. The iris made it possible to control how much light entered the cavity and hereby also with modes where present. When making the iris smaller we are sure that the resonances we see are due to the TEM00, because the intensity is largest at the center, as mentioned earlier. In Figure 12 the FSR of the cavity can be seen with and without sidebands. After minimizing the higher order modes the mirrors and the lenses were adjusted to maximize the transmission output.

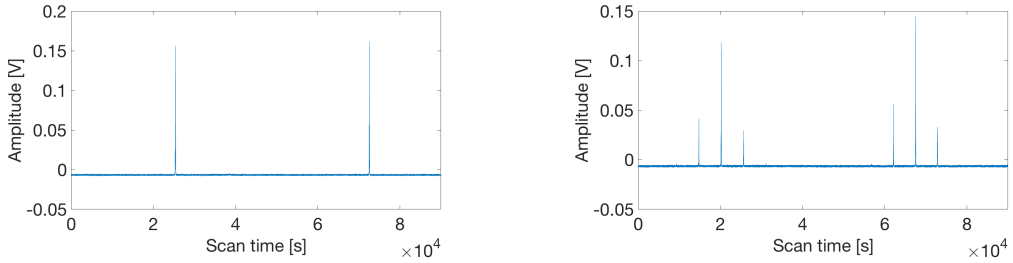

(a) (b)

Figure 12: The FSR (TEM00 modes) of the Fabry-Pérot interferometer (a) without sidebands and (b) with sidebands at 20MHz.

4.2.2 Results

For this part of the experiment the setup (B) in Figure 4 was used. We took a total of five measurements of the waveguide 83. In each measurement we scanned over a 100 nm interval, going from 1530 nm to 1630 nm. We scanned for a total time of 100 s with a scan speed of 1 nm/s. A typical scan of the fiber cavity, the Fabry-Pérot interferometer and the microresonator is depicted in Figure 13.

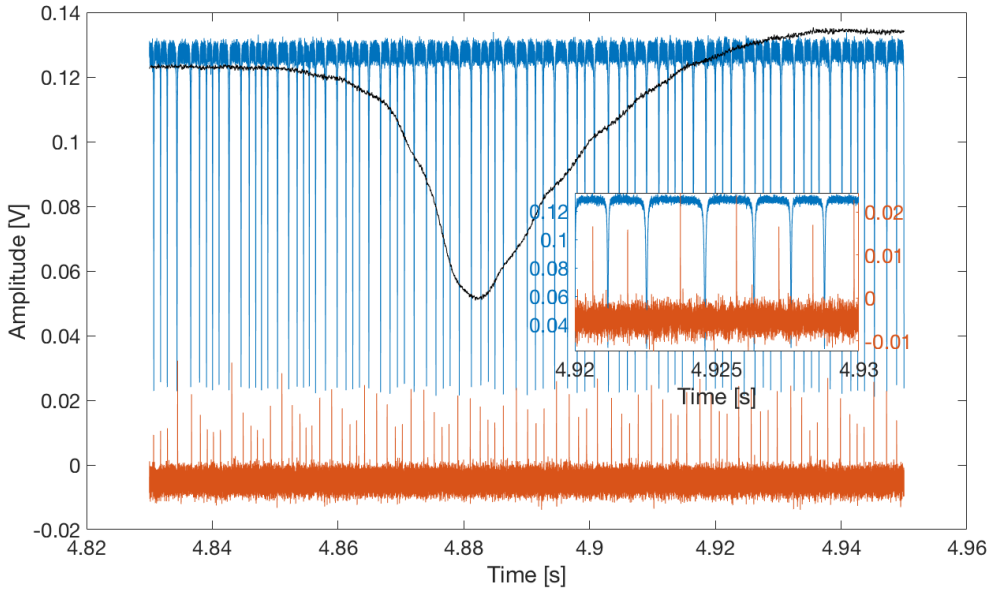

Figure 13: A section of a scan of the Fabry-Pérot interferometer, the microresonator and the fiber cavity measured simultaneously. The black curve is a single resonance of the microresonator. The blue data is the fiber cavity and the red is the Fabry-Pérot interferometer. A zoom in on the two cavities is shown in the subplot.

.

In the same way as with setup (A), in order for us to look at the dispersion of the microresonator, we need to find the FSR of the selfsame. However, with this setup it is somewhat simpler to calibrate going from scan speed in seconds to frequency in Hz. As mentioned before, the interferometer that we build has a well defined FSR determined using the sidebands created from an EOM. This means that we know the exact distance in frequency between each resonance from the scan over the Fabry-Pérot interferometer, namely 175.3 MHz. By locating each peak of the resonances the axis is, as with the acetylene cell, calibrated using the location of the resonance peaks. We know that from the first to the second resonance is one FSR, and from the second to the third there is two FSR and so forth. After the scan time has been calibrated to frequency, the FSR of the microresonator and the fiber cavity can be determined in the same way as done before. We locate each peak, now given in frequency, and the FSR is found trivially as the distance between each peak. With the Fabry-Pérot interferometer we obtain resonance much closer to each other than the lines in the spectrum were. With that many reference values, it is much more reasonable to assume a linear scan speed, as we have less spacing between the points. With a FSR of around 38 MHz we obtain around 69,000 resonances over a range of 100 nm instead of the 30 lines over a range of 50 nm for acetylene. The assumption that the laser is linear between two resonances is more justified in this case. The FSR of the microresonator as a function of the resonance number is shown in Figure 14.

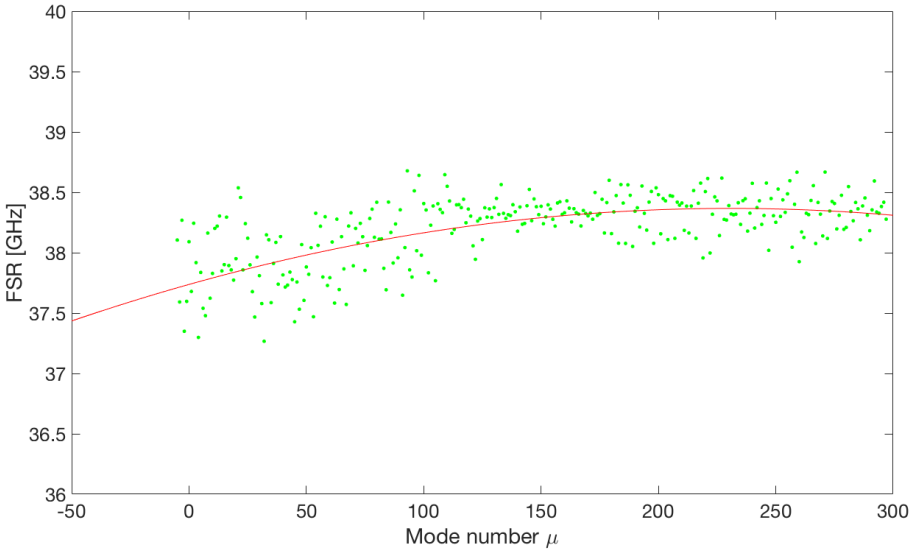

Figure 14: **FSR as a function of mode number** μ for a single scan. On the x-axis the mode numbers centered around the $\mu = 0$, located at 1542 nm, are plotted. On the y-axis we see FSR in GHz. The red line is a second order polynomial fit of the data points

.

The measured FSR is fitted with a second order polynomial, ax^2+bx+c, instead of using a linear fit, due to the tendency of the data points. As for the acetylene cell the parameters D_1 and D_2 are determined from the fitted curve. D_1 is the FSR corresponding to the mode number $\mu = 0$. For simplification the same wavelength was chosen for $\mu = 0$, 1542 nm, as for the setup with the acetylene cell. In this case the parameter D_2 is determined by the b-value of the polynomial fit. Some of the measurements are much better than the others due to noise from the laser and therefore only two of the initial five measurements have been included. The results can be seen in Table 3.

Table 3: Results

$\mathbf{D_1}$ **[rad/s]**	$\mathbf{D_2}$ **[rad/s]**	β_2 **[fs^2/mm]**
$2.3737 \cdot 10^{14} \pm 8.2938 \cdot 10^{11}$	$4.0871 \cdot 10^{7} \pm 6.9492 \cdot 10^{6}$	$-0.0510 \pm 8.6739 \cdot 10^{-3}$

4.2.3 The Fiber Cavity

Using the Fabry-Pérot interferometer that we built, we also found the FSR of the fiber cavity as seen in Figure 15. The reason behind this was to determine whether or not there was dispersion in the fiber cavity, but it is not clear from the measurements that we took. From the fit of the data points, we found the slope of the fit to be $(4.1985 \pm 1.7675) \cdot 10^{-8}$, which does indicate that the line has a slope, but it is far too small to conclude how much dispersion there is in the fiber cavity. What we do from Figure 15 is that the FSR seems to oscillate around a mean value which in this case is 169 MHz.

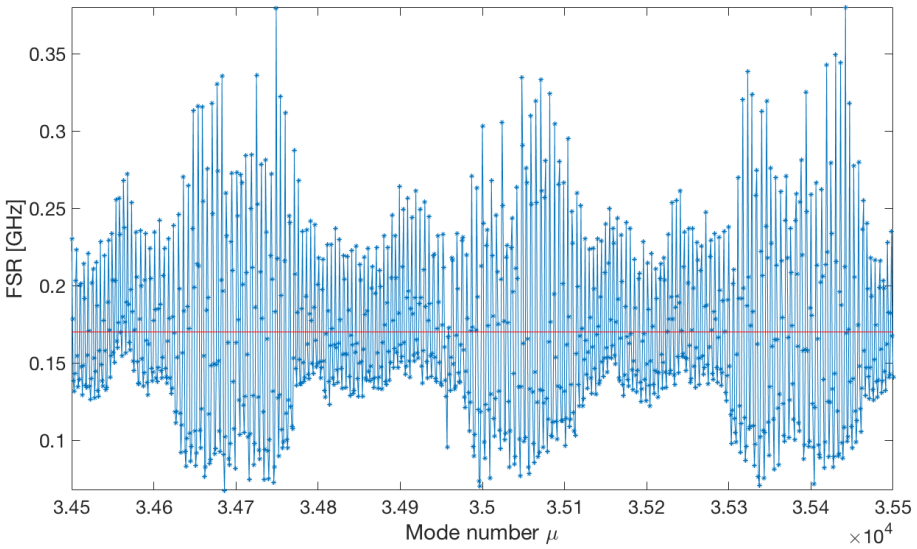

Figure 15: **A section of the FSR of the fiber cavity as a function of mode number** μ for a single scan. On the x-axis the mode numbers centered around the $\mu = 0$, located at 1542 nm, are plotted. On the y-axis we see FSR in GHz. The red line is a linear fit to the data points.

.

5 Discussion

The goal of the project was to examine the dispersion of an AlGaAs microresonator to see if a frequency comb could be achievable in the future. By scanning the microresonator along with a reference, the FSR could be measured and from here the GVD could be calculated.

In the first part of the experiment, the FSR was determined using an acetylene gas cell as a reference. The spectral lines of the molecular gas was used calibrate from scan time to wavelength. This method provided some good results, of which the peaks of the resonances very clearly stood out making it easy to locate each peak. However, for all the scan speeds, except 25 nm/s, we did not always find the same number of resonance in each scan. This could be a simulation error in the `findpeak` function in MATLAB used to find the resonance peaks, as the outliers are not caused by a physical phenomenon. Furthermore, as seen in Figure 8, the FSR values fluctuate around a mean value of 38,3 GHz. This fluctuation makes a fit of the values more uncertain, leading to a relatively high uncertainty of the D_2 parameter for all scan speeds. The four different scan speeds were also compared by looking at the standard deviation of the residuals for the FSR compared to the fit and by looking at the mean residual value, shown in Figure 2 and Figure 10. What we found, was that each scan speed provided more or less the same results and uncertainties for our final results. This would indicate that the scan speed, within this area, does not have a significant influence on the data from the measurements. Although, as mentioned, one could argue that the results of the 100 nm/s compared to the other scan speeds stands a bit out when looking at the residuals. The measurements conducted with a scan speed of 100

nm/s has more single outlying values when looking at the mean residuals. It also exhibits a somewhat larger standard deviation in the fifth scan than the rest of the scan speeds. From this it would seem that a lower scan speed would be preferable when conducting the measurements of the dispersion with this setup. Conclusively, the thing to consider most about the setup is that, although the spectral lines are known with good precision, we only have around 30 lines to calibrate after when converting the axis.

By using a Fabry-Pérot interferometer we can achieve a smaller FSR by buildning a long free space cavity. By having a free space cavity of the length that we had, very narrow spacing between each reference is achieved. This means that assuming that the laser is scanning linearly between each resonance is more reasonable more reasonable in this case, compared to when the same was done for the acetylene cell. Looking at the results for the dispersion, β_2, we see that using the Fabry-Pérot interferometer has markedly increased the results for the dispersion of the microresonator. For the acetylene reference we found the results to be very small compared to what was expected compared to the simulations made by Martin Romme Henriksen [17], seen in Figure 16.

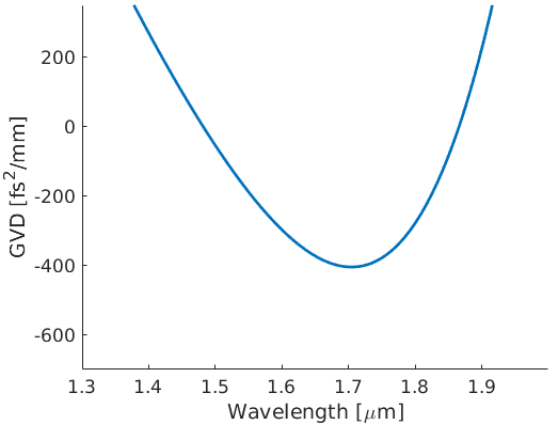

Figure 16: **Simulation taken from [17] of the GVD for waveguide 83** On the x-axis we have the wavelength and on the y-axis we see the expected GVD value in fs^2/mm.

This is due to the large spacing. We assumed the laser to scan linearly in between each reference line, but in reality the laser is not doing that. So, when the spacing is that large, the assumption no longer holds. From M. R. Henriksen's simulations we would expect a GVD of around -200 fs^2/mm. For the acetylene setup much more realistic values (-140 fs^2/mm) were achieved by looking at one FSR at a time over the whole scan. This supports the suspicion that the spacing of the acetylene cell is too great and motivates the idea of using the Fabry-Pérot interferometer. From the results of the Fabry-Pérot interferometer setup we did see that using the interferometer the results for the dispersion of the microresonator markedly increased. The problem is that the values obtained here seems a bit too small compared to simulations but nevertheless they are far more reasonable that the results obtained for acetylene.

When looking at the FSR we basically compare the frequency of the laser with the resonance of the cavity. From our results we see that the FSR of the microresonator and

the fiber cavity seems to be oscillating around a mean value that corresponds well with their supposed FSR of 38 GHz and 170 Mhz, respectively. There can be two plausible causes for this oscillating behaviour. One explanation could be that the oscillations were due to mechanical effects, but this seems rather unlikely. If mechanical effects were the cause it would mean that the optical path length (OPL) would oscillate, but since our microresonator is made of glass, the only thing that could affect the OPL is the temperature. Having the temperature cause periodic oscillations seems rather implausible and we therefore rule this out as the cause of the oscillations. We are then left with the other explanation, which would be that the frequency of the laser is not constant in time as we assumed when converting the scan time to frequency.

5.1 Further Work

After analyzing the results of the measurements for both the acetylene setup and for the setup with the Fabry-Pérot interferometer it is clear that the best results were obtained using the interferometer method. It could be interesting to try and work further with the free space cavity that we build. Better results could quite possibly be obtained if the finesse of the cavity could be reduced. One way of reducing the finesse is to try and change the high reflectance mirrors used with some of a lower reflectance. Also, the profile used to build our cavity was made of aluminum, which is very susceptible to changes in temperature. Even though we did not conduct a further examination, it is quite possible that temperature could have en influence on the FSR of the cavity as the OPL would change if the aluminum expanded/contracted.

6 Conclusion

In this thesis the dispersion of waveguide 83 on the AlGaAs microresonator CG49 has been measured using two different setups to determine the most optimal way of mapping the dispersion. In the first setup an acetylene cell was used as a reference and we found the dispersion to be of order 10^-3 fs^2/mm, which was somewhat smaller than the expected value of around -200 fs^2/mm. This was due to the spacing of the reference being too large for us to assume, that the laser was scanning linearly between two reference points. To reduce the spacing between the reference points, a Fabry-Pérot interferometer with a fixed FSR was built such that we increased the number of reference points by a order of 10^3 which made it much more reasonable to assume the laser scan being linear. Using this setup we obtained a dispersion value of $\beta_2 = -0.0510 \pm 8.6739 \cdot 10^{-30}$ fs^2/mm.

Bibliography

References

[1] Menlo Systens, *Optical Frequency Combs.* `http://www.menlosystems.com/products/optical-frequency-combs/`, date: 13JUN18.

[2] Yang Liu, Yi Xuan, Xiaoxiao Xue, Pei-Hsun Wang, Steven Chen, Andrew J. Metcalf, Jian Wang, Daniel E. Leaird, Minghao Qi, Andrew M. Weiner. *Investigation of mode coupling in normal-dispersion silicon nitride microresonators for Kerr frequency comb generation.* Optica, (2014).

[3] Govind P. Agrawal. *Nonlinear Fiber Optics.* Academic Press, , 3^{rd} Edition , 2001.

[4] R.G. Hunsperger. *Integrated Optics: Theory and Technology.* Springer, 5^{th} Edition, 2002.

[5] RP Photonics Encyclopedia, *Frequency Combs.* `https://www.rp-photonics.com/frequency_combs.html`, date: 09JUN18.

[6] Minhao Pu, Luisa Ottaviano, Elizaveta Semenova, Kresten Yvind. *Efficient frequency comb generation in AlGaAs-on-insulator.*. Optica, (2016).

[7] T. Herr, V. Brasch, J. D. Jost, I. Mirgorodskiy, G. Lihachev, M.L. Gorodetsky, T.J. Kippenberg. *Mode spectrum and temporal soliton formation in optical microresonators.* Physical Review Letter **113**, 123901 (2014).

[8] RP Photonics Encyclopedia, *Optical Resonators.* `https://www.rp-photonics.com/optical_resonators.html`, date: 28MAY18.

[9] RP Photonics Encyclopedia, *Free Spectral Range.* `https://www.rp-photonics.com/free_spectral_range.html`, date:28MAY18.

[10] Luisa Ottaviano, Minhao Pu, Elizaveta Semenova, Kresten Yvind. *Low-loss high-confinement waveguides and microring resonators in AlGaAs-on-insulator.* Optics Letters **3996**, 269558 (2016).

[11] BATOP Optoelectronics, *Refractive index n of AlGaAs* `https://www.batop.de/information/n_AlGaAs.html`, date: 10JUN18

[12] E.G. Grosche, J. Meissner. *Wavelength reference materials for optical telecommunications - development and characterization.* Physikalisch-Technische Bundesanstalt (Germany), Advanced Optics Solutions (Germany). `http://www.ursi.org/proceedings/procGA02/papers/p0600.pdf`, date: 11JUN18.

[13] Mitsuhiro Kusaba, Jes Henningsen. *The 1+3 and the 1+2+4+5 Combination Bands of 13C2H2. Linestrengths, Broadening Parameters, and Pressure Shifts.* Journal of Molecular Spectroscopy **209**, (2001)

[14] C. Latrasse, M. Breton, M. Têtu, N. Cyr, R. Roberge, B. Villeneuve. *C_2HD and $^{13}C_2H_2$ absorption lines near 1530 nm for semiconductor-laser frequency locking.* Optics Letters, (1994)

[15] Robert W. Boyd. *Nonlinear Optics.* Academic Press, 2^{nd} Edition, 2003.

[16] Ajoy Ghatak, K. Thyagarajan. *Introduction to Fiber Optics* Cambridge University Press, $1^{st} Edition, 2000$

[17] Simulations as part of the work done by Martin Romme Henriksen, Quantum Metrology group, Niels Bohr Institute, University of Copenhagen.

Appendix

A $^{13}C_2H_2$ Spectral Lines Values for the $\nu_1 + \nu_3$ Band [13].

Line	Wavelength nm
R0	1532.770122
R1	1532.254149
R2	1531.743568
R3	1531.238455
R4	1530.738888
R5	1530.244928
R6	1529.756624
R7	1529.274007
R8	1528.797150
R9	1528.325911
R10	1527.860440
R11	1527.400694
R12	1526.946678
R13	1526.498390
R14	1526.055848
R15	1525.619030
R16	1525.187963
R17	1524.762647
R18	1524.343090
R19	1523.929301
R20	1523.521288
R21	1523.119057
R22	1522.722618
R23	1522.332020
R24	1521.9471
R25	1521.5683
R26	1521.1950
R27	1520.8279
R28	1520.4662
R29	1520.1105
R30	1519.7608
R31	1519.4169
R32	1519.0788
R33	1518.7469
R34	1518.4204
R35	1518.0945
R36	1517.7854
R37	1517.4769
R38	1517.1735
R39	1516.8762
R40	1516.5850

Line	Wavelength nm
P1	1533.818025
P2	1534.349922
P3	1534.887155
P4	1535.429793
P5	1535.977916
P6	1536.531606
P7	1537.090932
P8	1537.655949
P9	1538.226691
P10	1538.803242
P11	1539.385463
P12	1539.973510
P13	1540.567350
P14	1541.166990
P15	1541.772436
P16	1542.383713
P17	1543.000806
P18	1543.623746
P19	1544.252541
P20	1544.887206
P21	1545.527755
P22	1546.174204
P23	1546.826568
P24	1547.484859
P25	1548.149138
P26	1548.819316
P27	1549.495492
P28	1550.177640
P29	1550.866180
P30	1551.560142
P31	1552.2604
P32	1552.9668
P33	1553.6786
P34	1554.3975
P35	1555.1221
P36	1555.8533
P37	1556.5894
P38	1557.3321
P39	1558.0820
P40	1558.8369